Molecular Layer Deposition of Alucone Polymer Films Using Trimethylaluminum and Ethylene Glycol

A. A. Dameron,[†,||] D. Seghete,[†] B. B. Burton,[†] S. D. Davidson,[‡] A. S. Cavanagh,[§] J. A. Bertrand,[†] and S. M. George*[,†,‡]

Department of Chemistry and Biochemistry, Department of Chemical and Biological Engineering, and Department of Physics, University of Colorado, Boulder, Colorado 80309

Received November 19, 2007. Revised Manuscript Received March 9, 2008

Polymeric films can be grown by a sequential, self-limiting surface chemistry process known as molecular layer deposition (MLD). The MLD reactants are typically bifunctional monomers for stepwise condensation polymerization and can yield completely organic films. The MLD of organic–inorganic hybrid polymers can also be accomplished using a bifunctional organic monomer and a multifunctional inorganic monomer. In this work, the growth of a poly(aluminum ethylene glycol) polymer is demonstrated using the sequential exposures of trimethylaluminum (TMA) and ethylene glycol (EG). These hybrid polymers, known as alucones, were grown over a wide range of temperatures from 85 to 175 °C. In situ quartz crystal microbalance and ex situ X-ray reflectivity experiments confirmed linear growth of the alucone film versus number of TMA/EG reaction cycles at all temperatures. The alucone growth rates decreased at higher temperatures. Growth rates varied from 4.0 Å per cycle at 85 °C to 0.4 Å per cycle at 175 °C. In situ Fourier transform infrared spectroscopy was used to monitor the surface reactions during alucone MLD. Ex situ FTIR spectroscopy, X-ray photoelectron spectroscopy, and X-ray reflectivity measurements were also employed to determine the chemical composition, thickness, and density of the alucone films. These ex situ studies revealed that the alucone films grown on Al_2O_3 ALD surfaces evolved under ambient conditions before reaching a stable state. Alucone films capped with rapid SiO_2 ALD displayed much more stability than alucone films grown on Al_2O_3 ALD surfaces. These results indicated that H_2O may facilitate the chemical transformation of the alucone MLD films. The alucone films represent a new class of organic–inorganic hybrid polymers. Modification of this basic alucone MLD chemistry with use of other diols or other bifunctional monomers can produce different alucone polymers with variable properties.

I. Introduction

Polymer films can be grown with molecular level control using molecular layer deposition (MLD) methods. In the past, organic polymer MLD has been accomplished using bifunctional organic monomers.[1] MLD growth has been demonstrated for a wide range of polymers such as polyamide,[2–4] polyimide,[5] polyimide−polyamide,[6] and polyurea.[7] The strategy for polymer MLD is similar to the methods employed for atomic layer deposition (ALD) of inorganic materials.[8,9] The MLD and ALD techniques are both based on sequential, self-limiting surface reactions. The ability to perform MLD for organic materials and ALD for inorganic materials suggests the extension of a hybrid MLD/ALD approach using organic and inorganic precursors for hybrid organic–inorganic film growth. The precursors for hybrid organic–inorganic polymer growth can be bifunctional organic monomers with various multifunctional organometallic precursors. One subset of these new reactions is based on the family of reactions that occurs between a metal alkyl and a diol (or glycol) organic molecule. The metal alkyl molecule is described by MR_x, and the diol is described by HO−R′−OH. The general MLD reactions between the metal alkyl and the diol can be written as follows:

$$MR^* + HOR'OH \rightarrow M-OR'OH^* + RH \quad (A)$$

$$R'OH^* + MR_x \rightarrow R'O-MR_{x-1}^* + RH \quad (B)$$

where the asterisks indicate the surface species. Both reactions A and B can be self-limiting. In reaction A, the reactions reach completion when all the MR* surface species

* Corresponding author. E-mail: Steven.George@Colorado.edu.
† Department of Chemistry and Biochemistry.
‡ Department of Chemical and Biological Engineering.
§ Department of Physics.
|| Present Address: Dynamic Organic Light, 2410 Trade Center Avenue, Longmont, CO USA 80503.

(1) Yoshimura, T.; Tatsuura, S.; Sotoyama, W. *Appl. Phys. Lett.* **1991**, *59*, 482.
(2) Adamczyk, N. M.; Dameron, A. A.; George, S. M. *Langmuir* **2008**, *24*, 2081.
(3) Du, Y.; George, S. M. *J. Phys. Chem. C* **2007**, *111*, 8509.
(4) Shao, H. I.; Umemoto, S.; Kikutani, T.; Okui, N. *Polymer* **1997**, *38*, 459.
(5) Putkonen, M.; Harjuoja, J.; Sajavaara, T.; Niinisto, L. *J. Mater. Chem.* **2007**, *17*, 664.
(6) Miyamae, T.; Tsukagoshi, K.; Matsuoka, O.; Yamamoto, S.; Nozoye, H. *Jpn. J. Appl. Phys. Part 1* **2002**, *41*, 746.
(7) Kim, A.; Filler, M. A.; Kim, S.; Bent, S. F. *J. Am. Chem. Soc.* **2005**, *127*, 6123.
(8) George, S. M.; Ott, A. W.; Klaus, J. W. *J. Phys. Chem.* **1996**, *100*, 13121.
(9) Ritala, M.; Leskela, M. Atomic Layer Deposition. In *Handbook of Thin Film Materials*; Nalwa, H. S., Ed.; Academic Press: San Diego, CA, 2001.

10.1021/cm7032977 CCC: $40.75
Published on Web 04/29/2008

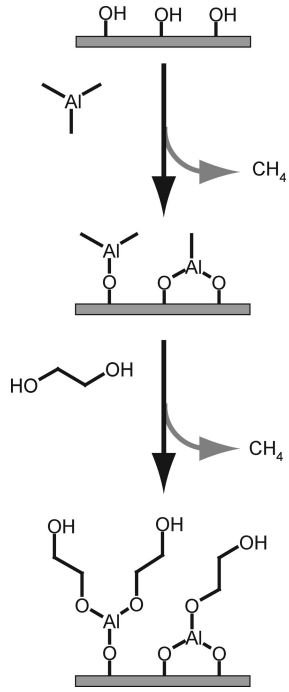

Figure 1. Schematic depicting alucone MLD growth. A hydroxylated surface is exposed to TMA and CH_4 is released as a product. The resulting surface is exposed to EG, CH_4 is again released as a product, and the surface is left covered with hydroxyl groups.

have been completely reacted. In reaction B, the reactions reach completion when all the R′OH* surface species have been completely reacted.

In this paper, we demonstrate this new hybrid organic–inorganic polymer MLD using the reaction of an aluminum-containing metal alkyl, $Al(CH_3)_3$ (trimethylaluminum (TMA)), with $HO-(CH_2)_2-OH$ (ethylene glycol (EG)). The sequential reactions of TMA and EG during MLD yields a polymeric film that can be approximately described as poly(aluminum ethylene glycol). A schematic illustrating the growth of poly(aluminum ethylene glycol) is shown in Figure 1.

There is earlier precedence for these hybrid organic–inorganic polymer materials based on the solution reaction of alkylaluminum molecules with an organic alcohol. Previous studies have demonstrated the formation of polymeric aluminum alkoxides with carbon-containing backbones and have called these materials "alucones".[10–13] These earlier alucones were formed by reacting diethylaluminum ethoxide with α,ω-diols such as ethylene glycol and catechol.[10,13,14] These previous solution studies determined the structure of the resulting polymers and used these alucones to fabricate γ-Al_2O_3.

The reaction between alkylaluminum molecules, such as TMA, and various diols have also been utilized to form alkylaluminum diolates.[15] The first alkylaluminum diolate was synthesized by the reaction of TMA and 1,2-di(hydroxymethyl)benzene.[16] These diolates are soluble cyclic products. In contrast, the alucones are organoaluminum oligomers that are insoluble in organic solvents. The first alucone was reported after the reaction of *cis*-but-2-ene-1,4-diols with TMA.[17] Subsequent solution studies also observed the formation of insoluble organoaluminum oligomers after the reaction of TMA with different aliphatic diols[18,19] and aromatic diols.[20] In contrast, this paper will demonstrate a gas phase MLD approach to fabricate alucone films.

The reaction illustrated by TMA + EG should be very general as a gas phase method to deposit organic/inorganic polymers by MLD. Many different metal alkyls based on various metals in the periodic table will react with diols to form the hybrid organic–inorganic composites. Many different diols exist where the organic R′ group can be varied to tune thin film properties. Consequently, there will be a very wide-ranging set of possible hybrid organic–inorganic films that will be possible by choosing different metal alkyls and various organic diols.[21]

II. Experimental Section

A. Chemicals and Materials. Alucone polymer films were grown using trimethylaluminum ($Al(CH_3)_3$; 97%, Sigma Aldrich) and ethylene glycol ($HO(CH_2)_2OH$; Reagent Plus >99%, Sigma Aldrich). Unless otherwise noted, the polymer films were grown on top of Al_2O_3 ALD layers. The alucone films were grown immediately following the deposition of the Al_2O_3 ALD layer using TMA and water (Optima grade, Fischer) by methods described previously.[8,22–24] The Al_2O_3 ALD layers were grown at the same temperatures as the alucone MLD films. Ultrahigh purity N_2 (Airgas) was used as the carrier gas in the viscous flow reactor and as the purge between reactant exposures.

For ex situ analysis, the films were grown on boron doped p-type Si(100) substrates with a thin native oxide (Silicon Valley

(10) McMahon, C. N.; Alemany, L.; Callender, R. L.; Bott, S. G.; Barron, A. R. *Chem. Mater.* **1999**, *11*, 3181.
(11) Rees, W. S.; Hesse, W. Preceramic Polymers for Aluminum Oxides. In *Chemical Perspectives of Microelectronic Materials II*; Interrante, L. V., Jenson, K. F., Dubois, L. H., Gross, M. E., Eds.; Materials Research Society: Pittsburgh, PA, 1991; p 563.
(12) Rees, W. S.; Hesse, W. Control Over Al_2O_3 Phase by Use of Polymer Precursors. In *Synthesis and Processing of Ceramics: Scientific Issues*; Rhine, W. E., Shaw, T. M., Gottschall, R. J., Chen, Y., Eds.; Materials Research Society: Pittsburgh, PA, 1992; p 51.
(13) Rees, W. S.; Hesse, W. Alucone Polymers And Their Pyrolytic Product Aluminum-Oxides. In *Inorganic And Organometallic Polymers II* ; ACS Symposium Series 572; American Chemical Society: Washington, DC, 1994; p 165.
(14) Atiya, G. A.; Grady, A. S.; Russell, D. K.; Claxton, T. A. *Spectrochim. Acta, Part A* **1991**, *47*, 467.
(15) Ziemkowska, W. *Coord. Chem. Rev.* **2005**, *249*, 2176.
(16) Pasynkiewicz, S.; Ziemkowska, W. *J. Organomet. Chem.* **1992**, *423*, 1.
(17) Pasynkiewicz, S.; Ziemkowska, W. *J. Organomet. Chem.* **1992**, *437*, 99.
(18) Ziemkowska, W.; Pasynkiewicz, S. *J. Organomet. Chem.* **1996**, *508*, 243.
(19) Ziemkowska, W.; Pasynkiewicz, S.; Kalbarczyk, E. *J. Organomet. Chem.* **1994**, *465*, 93.
(20) Ziemkowska, W.; Pasynkiewicz, S.; Skrok, T. *Main Group Met. Chem.* **1998**, *21*, 105.
(21) We initially reported our results on alucone MLD at the AVS Topical Conference on Atomic Layer Deposition (ALD2007) in San Diego, CA, in June 2007 (A. A. Dameron, S. D. Davidson, B. B. Burton, J. A. McCormick, A. S. Cavanagh, and S. M. George, "Molecular Layer Deposition of Alucone Polymer Films Using Trimethylaluminum and Ethylene Glycol", June 26, 2007). We note that we learned of work on similar hybrid organic/inorganic MLD films at the same meeting (O. Nilsen, University of Oslo, "Organic-Inorganic Hybrid Materials by Atomic Layer Deposition", June 26, 2007).
(22) Dillon, A. C.; Ott, A. W.; Way, J. D.; George, S. M. *Surf. Sci.* **1995**, *322*, 230.
(23) Elam, J. W.; Groner, M. D.; George, S. M. *Rev. Sci. Instrum.* **2002**, *73*, 2981.
(24) Groner, M. D.; Fabreguette, F. H.; Elam, J. W.; George, S. M. *Chem. Mater.* **2004**, *16*, 639.

Microelectronics, Inc.). Bulk analysis of alucone MLD films was also performed ex situ using Fourier transform infrared (FTIR) spectroscopy on dipolished Si(100) wafers (Institute of Electronic Materials Technology). Prior to deposition, each sample was first rinsed with water, acetone, and methanol, and then dried in an Ar stream.

For surface chemistry analysis by FTIR and for film thickness verification by transmission electron microscopy (TEM), the alucone MLD films were also grown on particles. These high surface area particle samples dramatically increase the signal-to-noise ratio and facilitate transmission FTIR investigations. The ZrO_2 particles (Sigma Aldrich) used for the FTIR studies had a diameter of ~30 nm. The $BaTiO_3$ particles (Ferro Electronic Materials, Niagara Falls, NY) employed for the TEM studies had a diameter of ~200 nm. The particles were pressed into a stainless steel grid (Etch Tech) for deposition in the ALD reactor.

B. Viscous Flow Reactor and Deposition Parameters. The viscous flow reactors used for these experiments were similar to reactors that have been described previously.[23] The FTIR experiments were performed in a viscous flow reactor equipped with an FTIR spectrometer.[3,25,26] The sample was placed in the reactor in a position that intersected the FTIR beam. The FTIR analysis can identify the surface species after each reactant exposure and can monitor the film growth versus the number of ALD cycles. All other experiments were performed in a larger viscous flow reactor. Alucone MLD growth was monitored at 85, 105, 135, 155, and 175 °C.

In all cases, the ALD and MLD films were fabricated by dosing the reactant precursors into the N_2 carrier gas. The amount of each precursor dose was controlled using pneumatic valves. The N_2 carrier gas was also used to purge the reactor between the precursor exposures. The Al_2O_3 was deposited using a 0.25 s TMA dose and a 0.15 s H_2O dose, with 60 s purge times between each TMA and H_2O dose. These dose times produced ~70–100 mTorr precursor pressure transients above the baseline pressure. For consistency, the same deposition and purge times were used at all temperatures for all experiments.

The alucone MLD films were deposited using a 0.5 s TMA dose and a 1.5 s EG dose, with a 120 s purge time between each TMA and EG exposure. These dose times produced ~130 mTorr TMA pressure transients and ~70 mTorr EG pressure transients above the baseline pressure. The quartz crystal microbalance (QCM) measurements determined that these dose times were more than sufficient to saturate the surfaces at all temperatures. Unless otherwise noted, the same deposition times were used at all temperatures for all experiments. The purge times were also long enough to ensure that no precursor was left in the reactor at the lower temperatures. The purge time also allowed the QCM to restabilize thermally before the next dose at the higher temperatures.

The rapid SiO_2 ALD films used for capping the alucone MLD films were grown using tris(*tert*-pentoxy)silanol (99.99%, Sigma-Aldrich).[27,28] The rapid SiO_2 ALD was performed using static exposures at 135 °C. After a N_2 purge and pumpdown, the gate valve to the pump was closed and TMA was dosed into the reactor using pneumatic valves for 0.45 s and allowed to react for 3 s. Following a 75 s pumpdown, the gate valve was closed again and the substrate was exposed to eight minidoses of tris(*tert*-pentoxy)-silanol. Each minidose of tris(*tert*-pentoxy)silanol consisted of dosing into the reactor for 1 s, reaction for 5 s, and subsequent pumpdown for 45 s. These tris(*tert*-pentoxy)silanol minidoses assured that the rapid SiO_2 ALD reaction chemistry reached completion. This procedure defined one rapid SiO_2 ALD cycle. The SiO_2 capping layer was grown using two rapid SiO_2 ALD cycles.

C. Quartz Crystal Microbalance Analysis. A detailed description of the QCM setup used for monitoring ALD has been described previously.[23] Briefly, the QCM measurements were performed in situ in the large viscous flow reactor using a Maxtek TM400 thin film deposition monitor. The QCM sensors were quartz crystals with a polished Au face and a 6 MHz oscillation frequency (Colorado Crystal Corp.). The crystals were sealed into a Maxtek BSH-150 bakeable crystal housing and purged during deposition to avoid growth on the back side. During growth, the QCM was positioned horizontally and facing downward in the middle of the reactor.

Before deposition of the alucone MLD films, at least 50 cycles of Al_2O_3 ALD were deposited on the crystal to ensure a reproducible starting surface. The observed Al_2O_3 ALD growth rates were also used to calibrate the mass gains observed during alucone growth. Both the Al_2O_3 ALD and the alucone MLD were deposited with a constant N_2 flow passing through the reactor. Additionally, the N_2 purge through the QCM housing generated an ~100 mTorr increase in the base pressure.

D. Fourier Transform Infrared Spectroscopy. Fourier transform infrared spectroscopic studies of the alucone films were performed using both in situ and ex situ analysis. The films were grown on dipolished Si wafers for the ex situ analysis at 105 and 155 °C. For each sample, 100 cycles of Al_2O_3 ALD followed by 150 cycles of alucone MLD were deposited on the Si wafers in the large viscous flow reactor. After deposition, the samples were removed from the reactor and transferred to the FTIR spectrometer for spectral examination. Samples grown using only 100 cycles of Al_2O_3 ALD prepared at the same temperatures provided the background reference spectra for the alucone spectra. The ex situ spectra were collected with a Nicolet 580 FTIR spectrometer.

The alucone films were deposited on ZrO_2 and $BaTiO_3$ particles in the FTIR reactor for the in situ analysis. The reactant exposures required for the reactions to reach completion on the particle surfaces were determined by alternately dosing small amounts of one precursor, purging, and then collecting the spectrum. Spectra were recorded after each precursor exposure to determine the changing surface species and after complete AB cycles to ensure that the film was growing. The in situ spectra were collected with a Nicolet 670 FTIR spectrometer operating with a nitrogen-cooled mercury cadmium telluride detector. Spectra were collected with a mirror speed of 1.8 $cm \cdot s^{-1}$ and averaged over 200 scans using 4 cm^{-1} resolution.

E. X-ray Reflectivity, X-ray Photoelectron Spectroscopy, and Transmission Electron Microscopy. X-ray reflectivity analysis was performed using a high resolution Bede D1 Diffractometer from Bede Scientific. The diffractometer was equipped with a Cu Kα X-ray tube with a 1.54 Å wavelength. A filament current of 40 mA and a voltage of 40 kV were used for the measurements. For each sample, a $\omega-2\theta$ scan was performed using a 10 arcsec step size and a 5 s acquisition time. The data were fit using the REFS fitting software from Bede Scientific to extract independently the thickness, density, and surface roughness of the thin films.

X-ray photoelectron spectra were acquired using a Perkin-Elmer 5600 photoelectron spectrometer with a monochromatic Kα source (12.5 mA, 12 kV) using a 1.1 μm diameter spot size and operating at a base pressure of 2×10^{-10} Torr. Survey spectra were acquired using a pass energy of 187 eV. High resolution spectra of the C 1s, O 1s, and Al 2p regions were collected with a pass energy of 23 eV. The binding energies were referenced to the adventitious C

(25) Du, X.; Du, Y.; George, S. M. *J. Vac. Sci. Technol., A* **2005**, *23*, 581.
(26) Du, Y.; Du, X.; George, S. M. *Thin Solid Films* **2005**, *491*, 43.
(27) Burton, B. B.; George, S. M. Unpublished results, 2007.
(28) Hausmann, D.; Becker, J.; Wang, S. L.; Gordon, R. G. *Science* **2002**, *298*, 402.

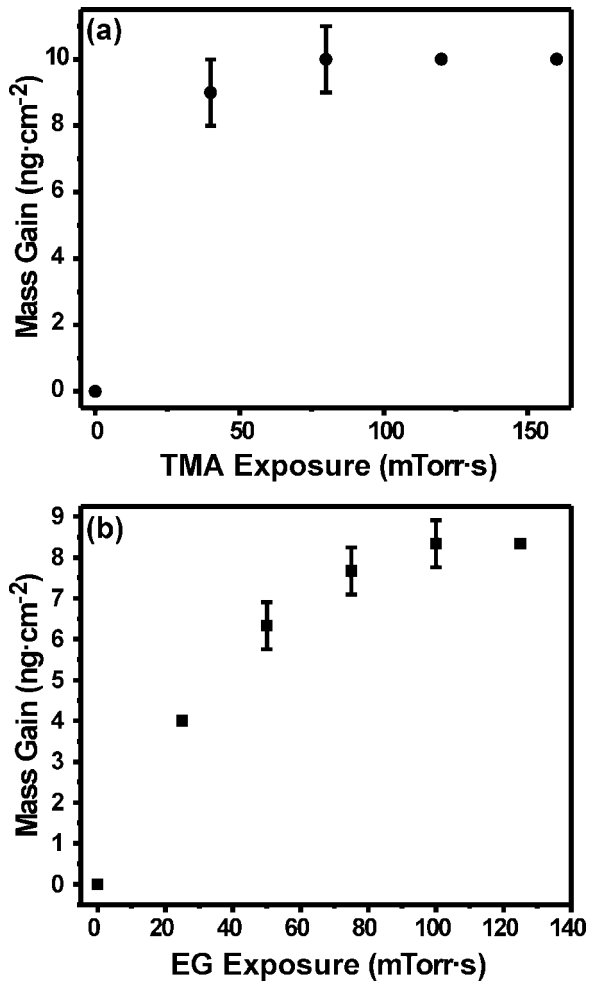

Figure 2. Mass gain versus reactant exposure for (a) TMA exposure and (b) EG exposure. In these experiments, one reactant exposure is varied while the other reactant exposure is held fixed at an exposure sufficient for completion of the reaction.

1s peak at 285 eV. All of the peaks were fit using Gaussian–Lorentzian line shapes and a linear background when necessary.

Images of the ALD and MLD films on the $BaTiO_3$ particles that were deposited during the FTIR experiments were obtained by TEM analysis. The nanoparticles were supported on a Formvar-coated copper grid. The TEM analysis was performed using a Philips CM10 transmission electron microscope with an 80 kV beam energy. The images were collected with a CCD camera mounted on the microscope.

F. Spectroscopic Ellipsometry. The index of refraction, *n*, and extinction coefficient, *k*, of the alucone films were obtained from ex situ reflective spectroscopic ellipsometry investigations. These measurements were performed using a rotating analyzer ellipsometer (J. A. Woollam, Lincoln, NE) that employs 44 wavelengths from 418.5 to 763.2 nm. The *n* and *k* values were derived from ellipsometric parameters for alucone MLD films grown at 135 and 155 °C on silicon substrates. The thicknesses of the alucone MLD layers used to derive the *n* and *k* values were determined by X-ray reflectivity (XRR) measurements.

III. Results and Discussion

A. Quartz Crystal Microbalance Analysis. Figure 2 displays the mass gains during TMA and EG exposures for steady state growth recorded by the in situ QCM at 135 °C.

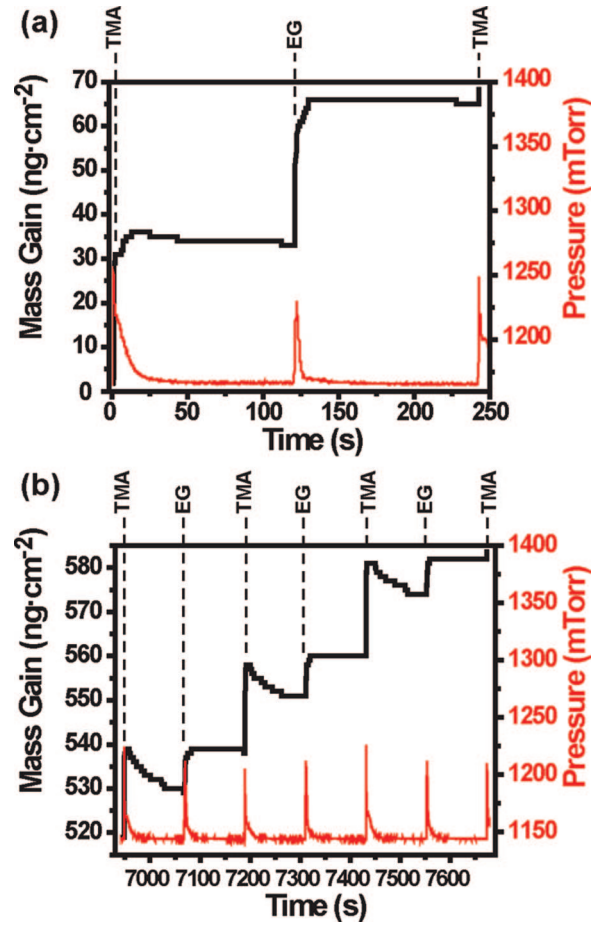

Figure 3. Mass gain and reactor pressure during sequential TMA and EG exposures. (a) The initial TMA and EG reaction cycle. (b) Three TMA and EG reaction cycles in the steady state regime showing the reproducibility of the mass gain for sequential TMA and EG exposures.

Similar curves were obtained at the other temperatures. The precursor exposures assume that the pressure results only from the dosed precursor. Both parts a and b of Figure 2 indicate that no further reaction occurs after the surface reaction reaches completion. The saturation point was observed after a 75 mTorr·s TMA exposure in Figure 2a. The saturation point was obtained after a 100 mTorr·s EG exposure in Figure 2b.

The in situ QCM analysis showed different mass gains per cycle for steady state growth and for the first cycle on an Al_2O_3 ALD surface at all deposition temperatures. Parts a and b of Figure 3 display mass gains versus time for the first cycle and for later cycles during steady state growth, respectively, at 135 °C. Although the mass gains varied with temperature, similar trends were observed at the other temperatures. In the first cycle on an Al_2O_3 ALD surface, as shown in Figure 3a, large positive gains were recorded that terminated at constant values for both TMA and EG. In contrast, the TMA exposures resulted in a mass gain and then a progressive decrease in mass gain after the TMA exposure during steady state growth, as shown in Figure 3b. The mass gain eventually reached a constant value during the steady state growth. The mass gains were observed to be consistent from cycle to cycle for both TMA and EG at all temperatures.

Table 1. Mass Gains after the TMA and EG Exposures during the First Cycle and during Steady State for Each Growth Temperature[a]

	mass gain per cycle during first cycle			mass gain per cycle during steady state growth			mass gain per cycle from linear fits
temp (°C)	ΔTMA	ΔEG	Δtotal	ΔTMA	ΔEG	Δtotal	Δtotal
85	28	48	76	24	32	56	58.2
105	33	36	69	23	17	40	39.4
135	32	34	66	10	8	18	18.2
155	28	42	70	10	4	14	14.5
175	30	46	76	7	2	9	8.8

[a] The last column displays the mass gains per cycle from the linear fits to the QCM data in Figure 4a.

The decrease in mass gain after TMA exposure occurred over a period of 60–90 s. This long progressive decrease is much longer than the time required for the TMA to return to the baseline pressure. Mass gains with decreases of this type have been observed previously during Al_2O_3 ALD on polymers.[29] This behavior is thought to result from TMA first being absorbed into the polymer and then slowly desorbing from the polymer after the TMA exposure. In contrast, the EG exposure resulted in a positive mass gain that reaches a plateau with a constant value. The change in the mass gains observed from the first cycle on the Al_2O_3 ALD surface to the steady state growth occurred over two to five cycles at all temperatures.

Table 1 presents the measured mass gains for all temperatures for the first cycle and for steady state growth. All the values are in units of ng·cm^{-2}. The mass gains per cycle decrease at higher temperatures in the steady state growth region. In contrast, the mass gains observed during the first cycle were nearly identical at all temperatures. Figure 4a shows the mass gain versus number of AB cycles for all temperatures. The growth rate decreases with temperature and is linear with the number of AB cycles for all temperatures. Each data set plot was fit to a line excluding the first 20 cycles. The growth rates per AB cycle from these fits are given in the last column of Table 1.

B. X-ray Reflectivity and Spectroscopic Ellipsometry Analysis. The temperature dependence of the growth rate was also observed by ex situ XRR analysis. Alucone MLD samples of varying thicknesses were grown and then analyzed for each deposition temperature. The alucone films were grown on Al_2O_3 ALD layers on Si wafers that had a native SiO_2 oxide. For each deposition temperature, alucone films were analyzed after 50, 75, 100, 150, and 200 AB cycles. Each resulting XRR scan was fit to account for the alucone MLD film, the Al_2O_3 ALD layer, and the native SiO_2 oxide film on the Si wafer. The results for film thickness versus number of AB cycles are shown in Figure 4b. There is excellent agreement between the linear alucone MLD film growth determined by the QCM measurements in Figure 4a and the XRR analysis in Figure 4b.

Figure 5 displays the growth per AB cycle and the film density for the various deposition temperatures determined by the XRR analysis. In agreement with the QCM measurements, the growth per cycle decreases with increasing temperature. The measured alucone film densities were independent of the deposition temperature and constant at ~1.5 g·cm^3. These measured densities of the alucone films

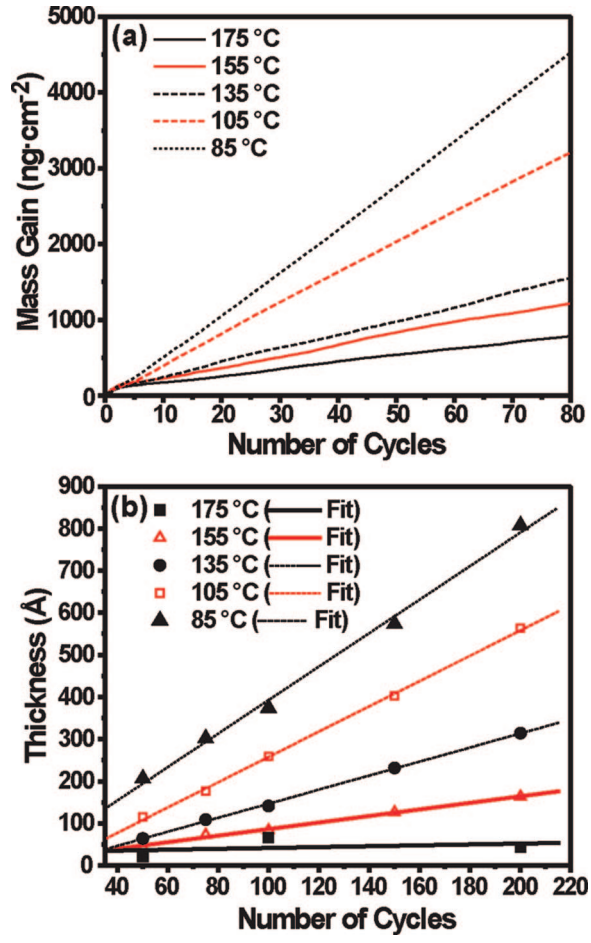

Figure 4. (a) Mass gain versus number of AB reaction cycles for a variety of deposition temperatures. (b) Film thickness measured using XRR versus number of AB reaction cycles for the same deposition temperatures.

are much less than the density of ~2.9 g·cm^3 for the Al_2O_3 ALD underlayer. Consequently, the film density must change very quickly at the interface between the Al_2O_3 ALD layer and the alucone MLD film. The details of the changing density at the interface may slightly affect the fits obtained by the XRR analysis.

The refractive indices of fresh alucone MLD films grown at 135 and 155 °C were $n = 1.507$ and $n = 1.512$, respectively. Both alucone films showed minimal absorption in the visible region. The extinction coefficients were $k = 0.0112$ and $k = 0.0114$, respectively. The refractive indices were also monitored during a 12 day period to determine the optical stability of the alucone MLD films. Over this time period, the n values for the two samples decreased less than 1% to $n = 1.497$ and $n = 1.494$, respectively, for films grown at 135 and 155 °C. Both samples also displayed a slight

(29) Wilson, C. A.; Grubbs, R. K.; George, S. M. *Chem. Mater.* **2005**, *17*, 5625.

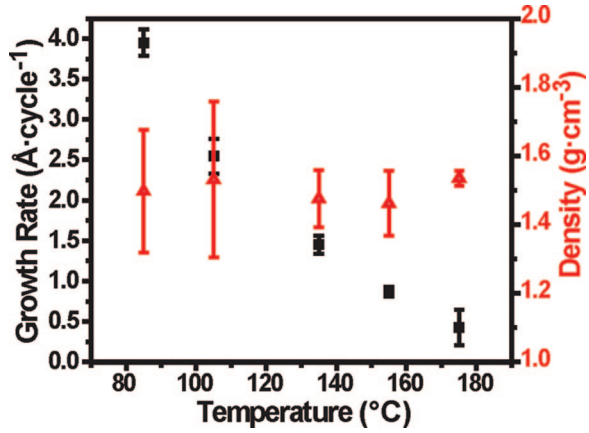

Figure 5. Growth per cycle and density for alucone MLD versus deposition temperature. The growth per cycle decreases at higher temperatures, and the density is constant at ~1.5 g·cm^3 versus temperature.

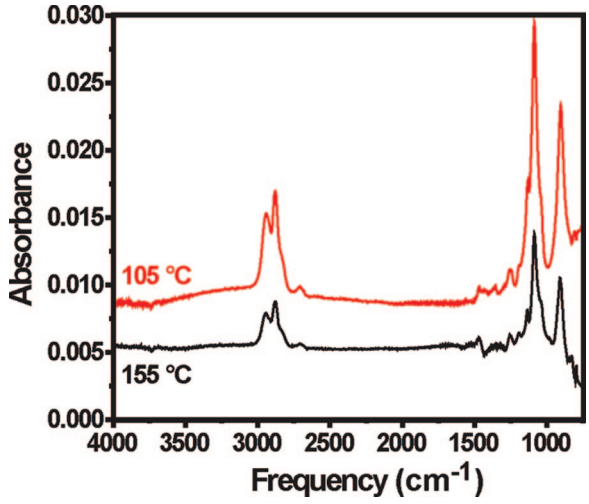

Figure 6. FTIR spectra of the alucone MLD films grown using 150 AB cycles at 105 and 155 °C. These difference spectra are referenced with respect to 100 AB cycle Al_2O_3 ALD films on SiO_2 substrates.

increase of their k values to $k = 0.0157$ and $k = 0.0201$, respectively.

C. Fourier Transform Infrared Spectroscopy. Ex situ FTIR difference spectra of alucone films grown using 150 AB cycles at 105 and 155 °C are shown in Figure 6. The spectra have been displaced for clarity in presentation. These alucone films were grown on Al_2O_3 ALD layers that were deposited using 100 AB cycles. These FTIR difference spectra were referenced to spectra of Al_2O_3 ALD layers grown using 100 AB cycles on the Si substrates at the same temperature. Large absorbances are observed at 2942 and 2879 cm^{-1}, corresponding to the CH_2 asymmetric and symmetric stretching vibrations. In addition, the C−C and the C−O stretching vibrations are observed at 1132 and 1086 cm^{-1}, respectively. The peak at 905 cm^{-1} is the Al−O stretching vibration in the alucone films.[30–32]

Table 2. Infrared Peak Assignments for the Bulk Alucone MLD Film Displayed in Figure 6 and the Surface Species Lost/Gained after the EG and TMA Reactions Shown in Figure 7

bulk peak position (cm^{-1})	surface peak position (cm^{-1})	appears after exposure to	assignment
~3300	~3300	EG	OH stretch
	2963	TMA	CH_3 asym stretch
2942	2956	EG	CH_2 asym stretch
	2928	TMA	CH_3 sym stretch
2879	2870	EG	CH_2 sym stretch
2708	2707	EG	combination
	1663	EG	
	1580	TMA	
	1538	TMA	
	1502	TMA	
1468			CH_2 scissor
	1439	TMA	CH_3 asym deform
1431			CH_2 wag, COH bend
1358			CH_2 twist, CH_2 wag, COH bend
1354			CH_2 twist, CH_2 wag, COH bend
1255			CH_2 twist, CH_2 wag
	1205	TMA	CH_3 sym deform
1192			CH_2 twist, CH_2 wag
1132	1135	EG	C−C stretch
1086	1100	EG	C−O stretch
905	910	EG and TMA	Al−O stretch

Peak positions and peak assignments for most of the observed absorbances are given in Table 2.[14,22,32–39] The observed vibrational features are consistent with the growth of the poly(aluminum ethylene glycol) polymer. All the main vibrational features are assigned to $-CH_2-$, C−O, or Al−O vibrational modes in alucone polymer. No peaks were observed from either CH_3 stretching vibrations or CH_3 deformations that would indicate any residual $-CH_3$ groups or unreacted TMA in the alucone films.

In situ FTIR analysis of alucone film growth on ZrO_2 particles at 135 °C also allowed for the surface species to be monitored after each A and B reaction. Figure 7 shows FTIR difference spectra of the surface after TMA exposure onto an EG-saturated surface (TMA−EG), and after EG exposure onto a TMA-saturated surface (EG−TMA). Each spectrum is referenced to the spectrum after the previous reaction. The spectra have been displaced for clarity in presentation. Positive changes in absorbance indicate species that were added to the surface. Negative changes in absorbance indicate species that were removed from the surface. Peak positions and peak assignments for most of the observed absorbances are also given in Table 2.

The CH_3 asymmetric and symmetric stretching vibrations at 2963 and 2928 cm^{-1}, respectively, and the CH_3 symmetric deformation mode at 1205 cm^{-1}, were the most prominent absorbances to increase after TMA exposure (TMA−EG)

(30) Fisher, G. L.; Walker, A. V.; Hooper, A. E.; Tighe, T. B.; Bahnck, K. B.; Skriba, H. T.; Reinard, M. D.; Haynie, B. C.; Opila, R. L.; Winograd, N.; Allara, D. L. *J. Am. Chem. Soc.* **2002**, *124*, 5528.
(31) Frank, M.; Wolter, K.; Magg, N.; Heemeier, M.; Kuhnemuth, R.; Baumer, M.; Freund, H. J. *Surf. Sci.* **2001**, *492*, 270.
(32) Liu, H.; Bertolet, D. C.; Rogers, J. W. *Surf. Sci.* **1995**, *340*, 88.
(33) Ferguson, J. D.; Weimer, A. W.; George, S. M. *Thin Solid Films* **2000**, *371*, 95.
(34) Hayes, N. W.; Beamson, G.; Clark, D. T.; Law, D. S. L.; Raval, R. *Surf. Interface Anal.* **1996**, *24*, 723.
(35) Kvisle, S.; Rytter, E. *Spectrochim. Acta, Part A* **1984**, *40*, 939.
(36) Matsuura, H.; Miyazawa, T. *Spectrochim. Acta, Part A* **1967**, *A 23*, 2433.
(37) Matsuura, H.; Miyazawa, T. *B. Chem. Soc. Jpn.* **1967**, *40*, 85.
(38) Matsuura, H.; Miyazawa, T.; Hiraishi, M. *Spectrochim. Acta, Part A* **1972**, *A 28*, 2299.
(39) Socrates, G. *Infrared Characteristic Group Frequencies*, 2nd ed.; John Wiley and Sons: Chichester, U.K., 1994.

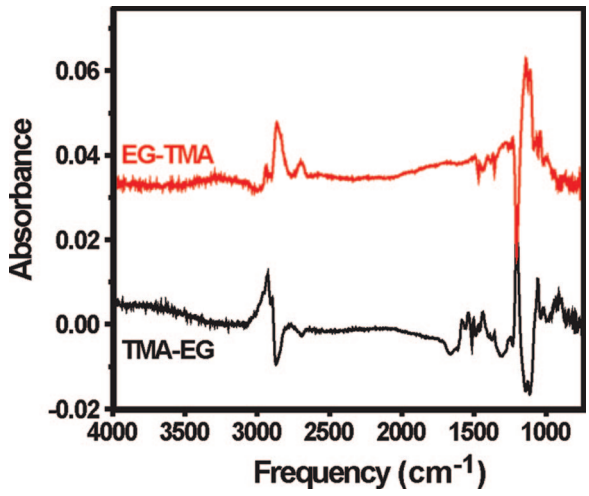

Figure 7. FTIR spectra after the EG and TMA surface reactions. TMA−EG is the spectrum after the TMA exposure minus the previous spectrum after the EG exposure. EG−TMA is the spectrum after the EG exposure minus the previous spectrum after the TMA exposure.

in Figure 7. These increases are consistent with $-AlCH_3$ species either on TMA molecules or on surface species deposited by TMA. There is also a decrease in absorbance observed for the CH_2 symmetric stretching vibration at 2870 cm^{-1}. This decrease could result from either a frequency shift of these vibrational modes or a removal of some $-CH_2-$ species during the TMA reaction. This removal could occur if TMA caused the cleavage of some $-O-CH_2-CH_2-$ species from the growing polymer film. In support of this possibility, the loss of absorbance for the C−O stretching vibration at 1100 cm^{-1} is also observed in Figure 7. This decreasing absorbance confirms that TMA can displace some $-O-CH_2CH_2-$ species.

The difference spectrum for TMA−EG in Figure 7 also does not reveal a significant loss of absorbance for O−H stretching vibrations at 3100–3600 cm^{-1}. This absence of a loss of O−H stretching vibrations is significant and suggests that the EG exposure does not yield the expected Al−O−CH_2CH_2−OH surface species predicted by the schematic in Figure 1. The absence of an absorbance loss for O−H stretching vibrations suggests that the EG reaction may react twice with $-AlCH_3$ species. This "double reaction" would remove the O−H stretching vibrations and produce Al−O−CH_2−CH_2−O−Al species. The "double reactions" could occur with either $-AlCH_3$ surface species or TMA molecules that may have absorbed into the growing polymer film.

A different mechanism for alucone MLD film growth is suggested by the absence of loss of absorbance for the O−H stretching vibration together with the QCM results in Figure 3b that show the ability of TMA to absorb into and then to desorb from the growing polymer. The polymer film may absorb TMA into the near-surface region of the polymer. The EG may then react primarily with the absorbed TMA molecules to form the alucone polymer. This reaction would be similar to chemical vapor deposition reactions between the reactant molecules expected for condensation polymerization. The TMA would then adsorb again into the near-surface region of the polymer to repeat the sequential reaction process.

The difference spectrum after the EG exposure (EG−TMA) in Figure 7 displays increases in the absorbances associated with CH_2 asymmetric and symmetric stretching vibrations at 2956 and 2870 cm^{-1}, respectively. Absorbance increases were also observed for the C−C and C−O stretching vibrations at 1100 cm^{-1}. These absorbance increases are consistent with the addition of $-OCH_2CH_2O-$ species. In addition, there is only a small absorbance increase for O−H stretching vibrations at 3100–3600 cm^{-1}. The lack of noticeable O−H stretching vibrations suggests once again that most of the EG molecules have reacted twice with $-AlCH_3$ species. In agreement with the reaction of $-AlCH_3$ species, there is a large decrease in the absorbance for the CH_3 symmetric deformation mode at 1205 cm^{-1}. A small decrease in the absorbance for CH_3 stretching vibrations was also observed at 2930−2960 cm^{-1}.

The self-limiting nature of the TMA and EG reactions was monitored by following the infrared absorption features versus time. The CH_3 symmetric deformation mode was used to monitor the TMA reaction. FTIR spectra were recorded progressively during a sequence of small TMA exposures. The integrated absorbance for the CH_3 deformation mode was determined over the region from 1166 to 1234 cm^{-1}. Figure 8a shows the normalized integrated absorbance as a function of TMA exposure. The integrated absorbance begins to decrease slightly after a TMA exposure of 250 mTorr·s exposure and has slowed considerably after a TMA exposure of 400 mTorr·s. The continued increase in absorbance suggests that TMA is still being absorbed into the polymer film in agreement with the QCM results in Figure 3b. The lack of a concurrent decreasing absorbance of the O−H stretching vibration argues that this TMA absorption results primarily from diffusion into the polymer film.

Figure 8b displays the normalized integrated absorbance as a function of the EG exposure. The CH_2 stretching vibrations were used to monitor the increase of $-OCH_2-CH_2O-$ species during the reaction. The CH_3 symmetric deformation mode was used to monitor the loss of $-AlCH_3$ species resulting from the EG reaction. Similar to Figure 8a, FTIR spectra were recorded progressively during a sequence of small EG exposures. The integrated absorbance was determined over the region from 2800 to 3000 cm^{-1} for the CH stretching vibrations and 1187 to 1247 cm^{-1} for the CH_3 deformation mode. Although there were also absorbances associated with CH_3 stretching vibrations in the 2800–3000 cm^{-1} region, the observed changes for the CH_2 stretching vibrations were much more dominant.

During the EG exposure, the integrated absorbance increased in the CH stretching vibration region and the integrated absorbance concurrently decreased in the CH_3 deformation region. After a 400 mTorr·s EG exposure, there were no additional absorbance changes. This behavior indicates that the EG reaction is self-limited by the reaction of all the $-AlCH_3$ species. Even though the majority of these $-AlCH_3$ species may be on TMA molecules, the limited number of TMA molecules absorbed in the polymer film yields a self-limiting EG reaction.

The FTIR results suggest a mechanism for alucone MLD film growth different from the mechanism shown in Figure

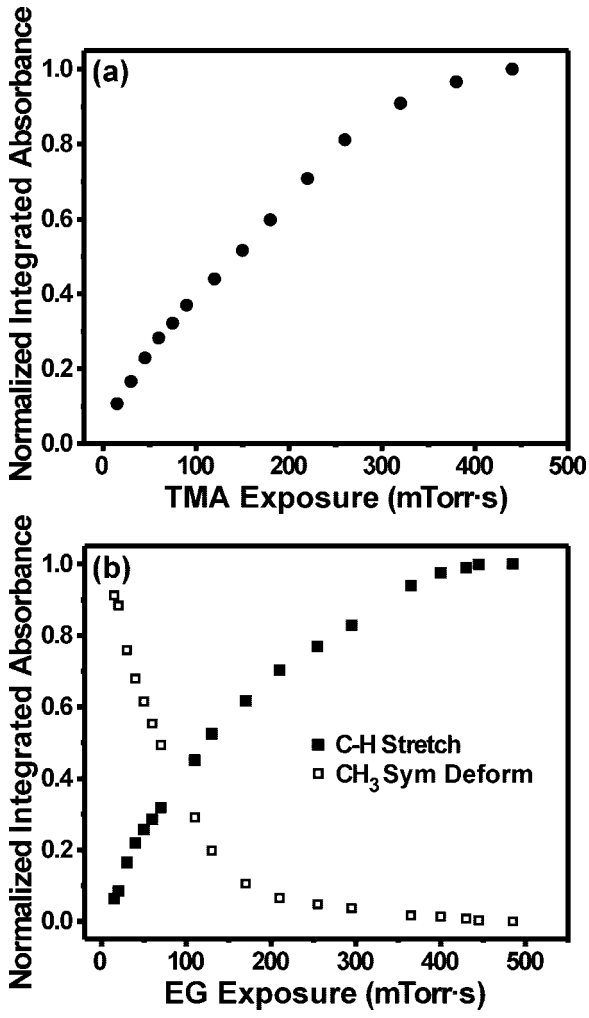

Figure 8. Normalized integrated absorbance of (a) CH_3 symmetric deformation mode versus TMA exposure and (b) C−H stretching vibration and CH_3 symmetric deformation mode versus EG exposure. The vibrational absorbance changes with exposure confirm the self-limiting nature of the TMA and EG reactions.

1. In addition to reacting with −OH species, TMA molecules may diffuse into the alucone polymer film. The EG molecules may then react with $-AlCH_3$ species both on the alucone polymer surface and on TMA molecules in the alucone polymer film. EG molecules may react twice because of the abundance of $-AlCH_3$ species. The reaction of EG with TMA molecules may be more appropriately described as a chemical vapor deposition reaction between EG and a finite number of TMA molecules in the near-surface region of the alucone MLD film. This proposed mechanism for alucone MLD film growth is pictured in Figure 9.

D. Transmission Electron Microscopy Analysis. Figure 10 displays a TEM image of a $BaTiO_3$ particle that was coated with 40 AB cycles of Al_2O_3 ALD and 50 AB cycles of alucone MLD at 135 °C. The image clearly shows a lighter contrast film on the darker contrast $BaTiO_3$ particle. The total film thickness on the $BaTiO_3$ particle was estimated to be ∼13 nm. The TEM image shows a contrast change in the film on the $BaTiO_3$ particle. The lighter contrast outer film on the $BaTiO_3$ particle is believed to correspond to the lower density alucone MLD film.

An Al_2O_3 ALD thickness of ∼6.5 nm after 40 AB cycles is consistent with an Al_2O_3 growth rate of 1.6 Å per cycle.

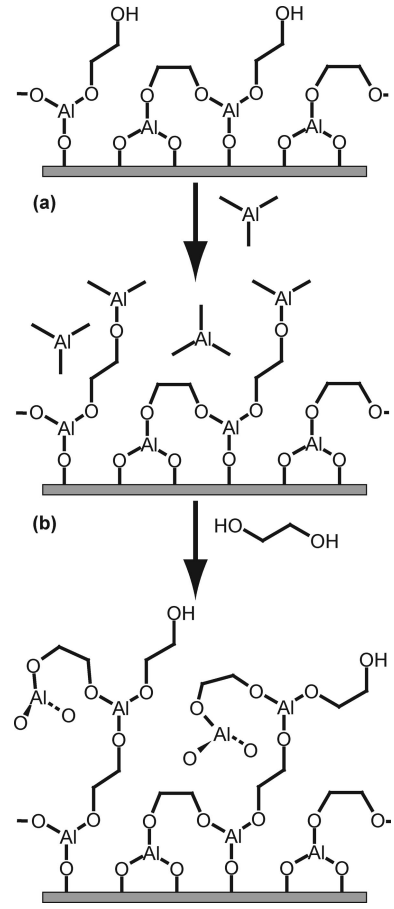

Figure 9. Schematic showing alternative alucone MLD growth mechanism. TMA can either react with −OH groups or diffuse into the alucone film. EG can react with one or two $-AlCH_3$ species on the alucone polymer or on TMA molecules in the alucone film. The solid arrows and dotted lines indicate bonds going out of or into the plane, respectively.

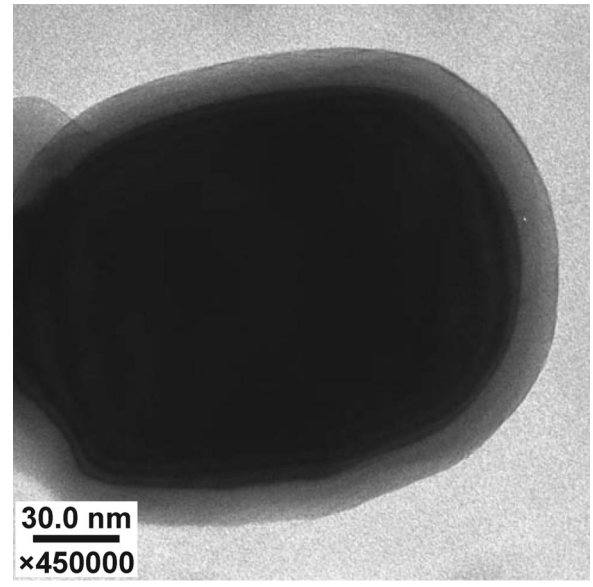

Figure 10. TEM image of a $BaTiO_3$ particle that was coated at 135 °C with 40 AB cycles of Al_2O_3 ALD and then 50 AB cycles of alucone MLD. The Al_2O_3 ALD and alucone MLD result in a ∼13 nm bilayer film thickness.

This growth rate is higher than growth rates of 1.2–1.3 Å per AB cycle for Al_2O_3 ALD on flat substrates. However, larger Al_2O_3 ALD growth rates are typically observed for

Al_2O_3 ALD on particles.[33,40] These larger growth rates are attributed to extra H_2O that is difficult to remove from particle beds because of low gas conductance. An alucone MLD thickness of ~6.5 nm after 50 AB cycles is consistent with an alucone MLD growth rate of 1.3 Å per cycle. This growth rate is in approximate agreement with the alucone MLD growth rates summarized in Figure 5.

The TEM image illustrates that sequential, self-limiting ALD and MLD reactions can produce very continuous and conformal films. The Al_2O_3 ALD and alucone MLD films are both very uniform in thickness and extremely conformal to the contours of the $BaTiO_3$ particle. This behavior has been observed previously for ALD on particles.[33,41–43] This TEM analysis extends this same behavior to MLD on particles. The alucone MLD on $BaTiO_3$ particles was deposited in a static particle matrix in this experiment. The MLD could also be performed in a fluidized particle bed reactor[44,45] or a rotary reactor[46,47] to agitate the particles to improve gas conductance and prevent particle agglomeration.

E. Stability of Alucone MLD Films. Figure 11a shows XRR scans of an alucone film grown using 150 AB cycles at 105 °C. The XRR scans were recorded at different time intervals after film fabrication. The scans reveal that the Bragg peaks move farther apart and shift toward higher angles with increasing time after film growth. The largest shifts were observed in the first 5–6 days after fabrication. Subsequently, the Bragg peak positions were very stable. A summary of the shift in the position of the Bragg peaks versus time is displayed in Figure 11b. The Bragg peaks result from interference caused by reflection from film interfaces. The Bragg peaks can be related to an overall film thickness. The change in the Bragg peak position is consistent with a film thickness decrease of ~22%.

In addition to the film thickness decrease, the alucone films also changed their chemical composition versus time. Figure 12 shows the FTIR difference spectra of alucone films grown using 150 AB cycles at 105 and 155 °C after aging for 2 months at room temperature in ambient air after fabrication. The FTIR difference spectra show the change of the FTIR spectra for the aged samples minus the original FTIR spectra immediately after fabrication. The FTIR spectra change significantly with time. However, the difference spectra for the alucone films grown at 105 and 155 °C are similar to each other. This similarity indicates that the same changes are occurring in both films.

The FTIR difference spectra reveal that vibrational features have appeared in both the O−H stretching region at 3500−3600 cm^{-1} and the C−H stretching region at 2800–3000 cm^{-1}. In addition, there is a broad peak at 1615 cm^{-1}, two overlapping peaks centered around 1425 cm^{-1}, and a strong peak at 1259 cm^{-1}. There are also strong overlapping absorbances at lower frequencies in the C−C, C−O, and Al−O stretching vibration regions.

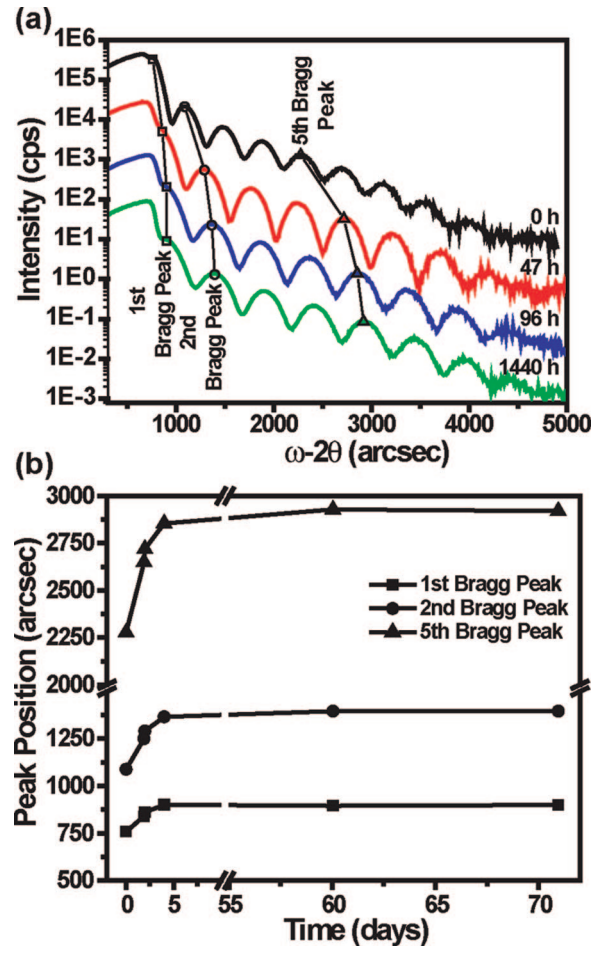

Figure 11. (a) XRR scans of an alucone MLD film prepared using 150 AB cycles at 105 °C on Al_2O_3 ALD films that were recorded at 0, 47, 96, and 1440 h after fabricating the film. The individual scans are offset for clarity. (b) Bragg peak positions for the first, second, and fifth Bragg peaks at different time intervals.

The peaks at 1615 and 1259 cm^{-1} correlate with C=C and C−O vibrational stretches and can be partially attributed to a enolate-type vinyl ether species in the form of CH_2=CH−O−Al.[48] This vinyl ether species could be formed by dehydration of the HO−CH_2−CH_2−O−Al species. Earlier studies have shown that alumina is an effective dehydration catalyst.[49,50] An earlier study of EG on an alumina supported copper surface identified vibrational features assigned at 1595 and 1270 cm^{-1} to CH_2=CH−O−Al.[48] The overlapping peaks around 1425 cm^{-1} are also consistent with =CH_2

(40) Ferguson, J. D.; Weimer, A. W.; George, S. M. *Chem. Mater.* **2004**, *16*, 5602.
(41) Ferguson, J. D.; Smith, E. R.; Weimer, A. W.; George, S. M. *J. Electrochem. Soc.* **2004**, *151*, G528.
(42) Ferguson, J. D.; Weimer, A. W.; George, S. M. *Thin Solid Films* **2002**, *413*, 16.
(43) Ferguson, J. D.; Yoder, A. R.; Weimer, A. W.; George, S. M. *Appl. Surf. Sci.* **2004**, *226*, 393.
(44) Wank, J. R.; George, S. M.; Weimer, A. W. *Powder Technol.* **2004**, *142*, 59.
(45) Wank, J. R.; George, S. M.; Weimer, A. W. *J. Am. Ceram. Soc.* **2004**, *87*, 762.
(46) McCormick, J. A.; Cloutier, B. L.; Weimer, A. W.; George, S. M. *J. Vac. Sci. Technol., A* **2007**, *25*, 67.
(47) McCormick, J. A.; Rice, K. P.; Paul, D. F.; Weimer, A. W.; George, S. M. *Chem. Vap. Deposition* **2007**, *13*, 491.
(48) Jobson, E.; Baiker, A.; Wokaun, A. *Ber. Bunsen-Ges. Phys. Chem.* **1989**, *93*, 64.
(49) deMiguel, S. R.; Martinez, A. C.; Castro, A. A.; Scelza, O. A. *J. Chem. Technol. Biotechnol.* **1996**, *65*, 131.
(50) Makgoba, N. P.; Sakuneka, T. M.; Koortzen, J. G.; van Schalkwyk, C.; Botha, J. M.; Nicolaides, C. P. *Appl. Catal., A: Gen.* **2006**, *297*, 145.

scissors vibrational modes. Vinyl CH_2 scissors features are typically observed at ~1440 cm^{-1}.[51]

The 1615 cm^{-1} peak can also be partially attributed to the scissors mode of adsorbed H_2O.[48] The O−H stretching vibrations at 3500–3600 cm^{-1} are also consistent with adsorbed H_2O or additional hydroxyl groups in the alucone film. This H_2O may result from the absorption of H_2O from the air or the formation of H_2O by dehydration of the adsorbed EG species. The additional hydroxyl groups may also result from enol species that may result from the dehydrogenation of adsorbed HO−CH_2−CH_2−O−Al species to form HO−CH=CH−O−Al species and H_2. Alumina can act as a dehydrogenation catalyst.[52,53] However, there is no strong evidence for a significant transformation from the enol form to the keto form because there is negligible vibrational absorbance at 1700–1750 cm^{-1} for the C=O carbonyl stretch.

To confirm the oxidation state of carbon in the alucone films, XPS spectra were recorded for samples grown at various temperatures. These alucone MLD films were grown using 100 AB cycles of TMA and EG on Al_2O_3 ALD layers on Si wafers at 85, 105, 135, 155, and 175 °C. The Al_2O_3 ALD layers were grown using 100 AB cycles of TMA and EG at the same temperatures as those used for the alucone films. XPS survey spectra revealed peaks from only carbon, oxygen, and aluminum. High resolution spectra were obtained for the C 1s, O 1s, and Al 2p regions. For each sample, the O 1s and Al 2p peaks were each fit with one Gaussian: Lorentzian (70:30) line shape. In contrast, the C 1s peaks required three Gaussian-Lorentzian line shapes to fit the peaks. The lowest energy C 1s peak assumed to be from adventitious C−H species was set to 285 eV to calibrate the other peaks.[30,54–58]

The O 1s and Al 2p peaks were observed at ~532 eV and ~74 eV, respectively. These peaks are similar in energy to the peak energies observed for Al_2O_3 films.[59] Figure 13 shows XPS spectra for the C 1s peak for alucone MLD films that were grown using 100 AB cycles at 105 and 155 °C. These films were analyzed after 6 and 35 days, respectively. The C 1s signal at the lowest energy peak at 285 eV is attributed to adventitious C−H species. The C 1s middle energy peak with a binding energy of ~286.5 eV is attributed to C−O species.[30,54–58,60] Both of these peaks are expected in the alucone MLD films.

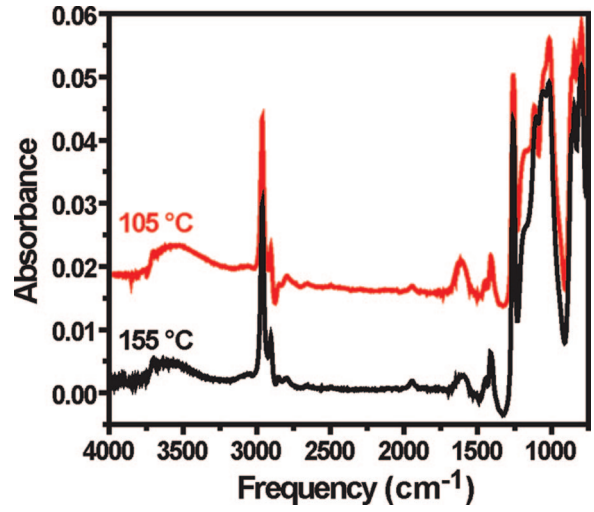

Figure 12. FTIR spectra of alucone MLD film prepared using 150 AB cycles at 105 and 155 °C after aging for 2 months. The difference FTIR spectra are referenced using the FTIR spectra shown in Figure 6.

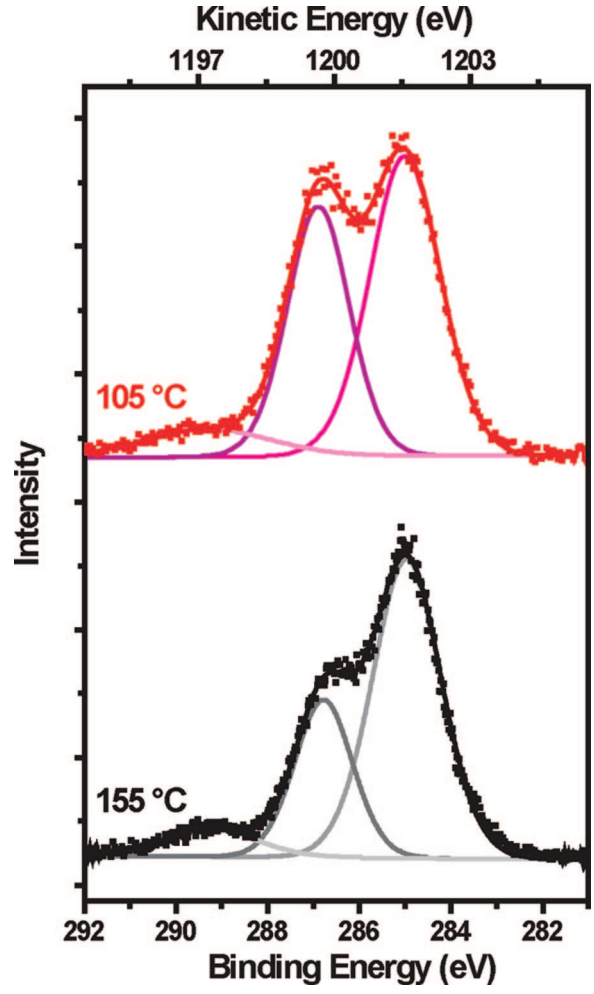

Figure 13. High resolution XPS spectra in the C 1s region for alucone MLD films grown using 100 AB cycles at 105 and 155 °C that were recorded after 6 and 35 days, respectively.

A third small C 1s peak was also observed with a binding energy of ~289 eV. XPS peaks with this energy are normally associated with highly electron withdrawing C=O groups.[54,56,60] However, there should be no C=O species in the alucone film assuming a growth mechanism similar

(51) Colthup, N. B.; Daly, L. H.; Wiberley, S. E. *Introduction to Infrared and Raman Spectroscopy*; Academic Press, Inc.: New York, 1975.
(52) Cordi, E. M.; Falconer, J. L. *J. Catal.* **1996**, *162*, 104.
(53) Cordi, E. M.; Falconer, J. L. *Appl. Catal., A: Gen.* **1997**, *151*, 179.
(54) Beamson, G.; Briggs, D. *High Resolution XPS of Organic Polymers: The Scienta ESCA 300 Database*; John Wiley and Sons: Chichester, U.K., 1992.
(55) Bebin, P.; Prud'homme, R. E. *Chem. Mater.* **2003**, *15*, 965.
(56) Briggs, D. *Surface Analysis of Polymers by XPS and Static SIMS*; Cambridge University Press: Cambridge, U.K., 1998.
(57) Popat, K. C.; Mor, G.; Grimes, C.; Desai, T. A. *J. Membr. Sci.* **2004**, *243*, 97.
(58) Popat, K. C.; Sharma, S.; Desai, T. A. *J. Phys. Chem. B* **2004**, *108*, 5185.
(59) Wagner, C. D.; Riggs, W. M.; Davis, L. E.; Moulder, J. F. *Handbook of X-ray Photoelectron Spectroscpy*; Muilenburg, G. E., Ed.; Perkin Elmer Corporation: Eden Prairie, MN, 1979.
(60) Silvain, J. F.; Arzur, A.; Alnot, M.; Ehrhardt, J. J.; Lutgen, P. *Surf. Sci.* **1991**, *251*, 787.

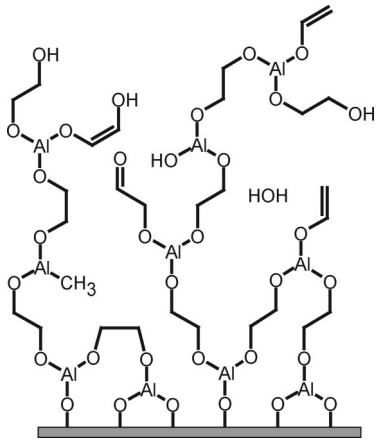

Figure 14. Illustration of aged alucone MLD film that is consistent with the absorbances in the FTIR difference spectra in Figure 12 and carbon chemical shifts in the XPS results in Figure 13.

to the mechanism shown in Figure 1. One possibility is that the AlO_x species in the alucone film facilitates the dehydrogenation of HO−CH_2−CH_2−O−Al species to produce HO−CH=CH−O−Al enol species and H_2. The enol species could then rearrange to produce an O=CH−CH_2−O−Al keto species. A C=O species could also be created by oxidation of the alcohol. Alumina can act as a catalyst for glycol oxidation to aldehyde.[48,61] However, the absence of infrared features in the 1700–1750 cm^{-1} region suggests that this oxidation reaction is minor or that the C=O stretching frequency is significantly perturbed by binding to AlO_x species in the alucone layer.[61]

Figure 14 shows a depiction of the aged alucone MLD film that is consistent with the absorbances in the FTIR difference spectra in Figure 12 and carbon chemical shifts in the XPS results in Figure 13. Based on the alternative mechanism for alucone MLD presented in Figure 9 and the chemical changes occurring with aging that are illustrated in Figure 14, the alucone MLD cannot be considered to be simply poly(aluminum ethylene glycol) or $(Al-OCH_2-CH_2O)_n$. The exact identity of the alucone MLD film requires additional analysis.

Because Al_2O_3 is catalytically active, alucone MLD layers were also grown directly on SiO_2 substrates using 100 AB cycles at 135 °C. The stability of the alucone layer was then monitored using XRR. XRR scans of the alucone MLD layer immediately after growth and then after 30 and 150 h are shown in Figure 15a. Unlike the alucone MLD layers grown on Al_2O_3 ALD, these layers could be fit very accurately to obtain film thicknesses. The film thickness decreased with time as shown in Figure 15b. The alucone MLD layer thickness decreased approximately 20% after 200 h and then was stable versus additional time.

Alucone MLD layers were also grown directly on SiO_2 substrates using 100 AB cycles at 135 °C and then capped with a SiO_2 layer using rapid SiO_2 ALD.[27,28] The rapid SiO_2 ALD was performed using tris(*tert*-pentoxy)silanol as the silanol precursor and trimethylaluminum (TMA) as the initiator at 135 °C. The stability of the alucone layer was

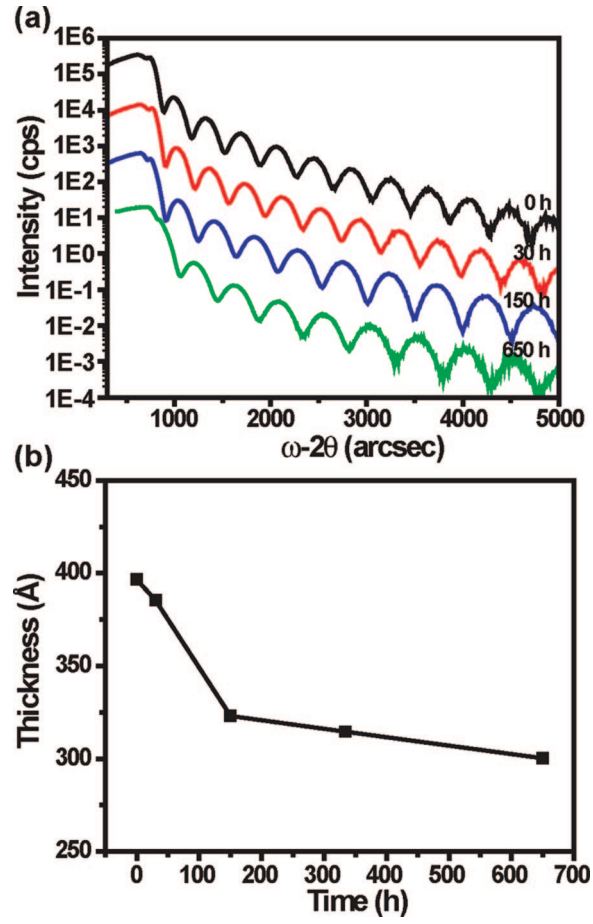

Figure 15. (a) XRR scans of an alucone MLD film prepared using 100 AB cycles at 135 °C on SiO_2 substrates that were recorded initially after fabrication and after 30, 150, and 650 h. The individual XRR scans are offset for clarity. (b) Thickness of the alucone MLD film versus time after fabrication.

again monitored using XRR. XRR scans of the alucone MLD layer immediately after growth and then after 430 h were almost identical and yielded the same film thickness. This lack of change indicates that the rapid SiO_2 ALD layer stabilizes the alucone layer presumably by preventing H_2O from diffusing into the film.

The ability of ALD layers to serve as gas diffusion barriers has been demonstrated in several recent studies. Low water vapor transmission rates (WVTRs) of $\sim 1 \times 10^{-3}$ $g/m^2/day$ have been obtained with 25 nm of Al_2O_3 ALD on Kapton and polyethylenenaphthalate (PEN).[62] These WVTRs are approximately 1000 times lower than the uncoated polymers. Even lower WVTRs of $\sim 1 \times 10^{-4}$ $g/m^2/day$ were measured with a bilayer of 25 nm of Al_2O_3 ALD and 65 nm of rapid SiO_2 ALD on Kapton.[63] Although the barrier properties of rapid SiO_2 ALD are not as effective as Al_2O_3 ALD, measurements of rapid SiO_2 ALD layer by itself lowered the H_2O permeability approximately 10 times and yielded a WVTR of $\sim 1 \times 10^{-1}$ $g/m^2/day$ on Kapton.[63] The rapid SiO_2 ALD layer on the alucone film may restrict the diffusion of H_2O and prevent the subsequent changes observed in the uncapped alucone layers.

(61) Bulushev, D. A.; Paukshtis, E. A.; Nogin, Y. N.; Balzhinimaev, B. S. *Appl. Catal., A: Gen.* **1995**, *123*, 301.
(62) Groner, M. D.; George, S. M.; McLean, R. S.; Carcia, P. F. *Appl. Phys. Lett.* **2006**, 88.
(63) Dameron, A. A.; Davidson, S. D.; Burton, B. B.; Carcia, P. F.; McLean, R. S.; George, S. M. *J. Phys. Chem. C*, in press.

IV. Conclusions

The growth of hybrid organic–inorganic alucone MLD layers was demonstrated using the sequential deposition of TMA and EG. The alucone MLD films were deposited at temperatures ranging from 85 to 175 °C. In situ quartz crystal microbalance and Fourier transform infrared spectroscopy, and ex situ FTIR, X-ray reflectivity, X-ray photoelectron spectroscopy, and transmission electron microscopy techniques were used to analyze the resulting films. The analysis indicated that the TMA and EG surface reactions were saturating and self-limiting. The alucone MLD film growth was linear with the number of AB cycles. The alucone MLD film growth rate decreased with increasing temperatures. The growth rates were 4.0 Å per cycle at 85 °C and decreased to 0.4 Å per cycle at 175 °C. The measured density was ~1.5 $g \cdot cm^{-3}$ for all the alucone MLD films.

The FTIR and QCM results suggested an alternative mechanism for alucone MLD film growth that expands upon the traditional view of self-limiting surface reactions. During alucone MLD, TMA molecules may diffuse into the alucone polymer film in addition to reacting with −OH species. The EG molecules may then react with $-AlCH_3$ species both on the alucone polymer surface and on TMA molecules in the alucone polymer film. The absence of absorbance for O−H stretching vibrations after the EG exposure suggests that EG molecules may react twice because of the abundance of $-AlCH_3$ species. This reaction of EG with TMA molecules is similar to a chemical vapor deposition reaction between EG and TMA molecules in the alucone MLD film.

Although the alucone MLD was very robust, the resulting alucone MLD films were unstable. The alucone film thickness decreased with time over the first 150 h after fabrication. The film shrinkage was also accompanied by chemical changes in the alucone that were consistent with either dehydration or dehydrogenation reactions. These results suggest that the catalytic properties of the AlO_x species in the alucone film may chemically alter the alucone MLD films. These reactions may be initiated by H_2O because alucone MLD films capped with rapid SiO_2 ALD layers did not display any film shrinkage.

This study demonstrates the fabrication of hybrid organic–inorganic alucone polymer films using MLD methods. Modifying this basic chemistry with the use of other diols should allow the tuning of the alucone polymer properties. Combination of different ALD and MLD surface chemistries may provide a wide variety of organic–inorganic films. These various organic–inorganic films will greatly expand the number and type of films that can be deposited using ALD and MLD methods. The physical and chemical instability of the alucone films may restrict their applications unless they can be stabilized with capping layers that are believed to prevent H_2O diffusion into the alucone films.

Acknowledgment. This work was supported by the National Science Foundation (CHE-0715552). Additional personnel funding was obtained from DARPA/MTO, SPAWAR (Contract No. N66001-07-1-2033). Some of the equipment used in this research was provided by the Air Force Office of Scientific Research. The authors thank Dr. Jarod A. McCormick for assistance with the XPS analysis and Dr. Thomas Giddings for assistance with the TEM analysis.

CM7032977